ARTICLES

Controlled nanoscale doping of semiconductors via molecular monolayers

JOHNNY C. HO[1,2]*, ROIE YERUSHALMI[1,2]*, ZACHERY A. JACOBSON[1,2], ZHIYONG FAN[1,2], ROBERT L. ALLEY[1] AND ALI JAVEY[1,2]†

[1]Department of Electrical Engineering and Computer Sciences, University of California at Berkeley, Berkeley, California 94720, USA
[2]Materials Sciences Division, Lawrence Berkeley National Laboratory, Berkeley, California 94720, USA
*These authors contributed equally to this work
†e-mail: ajavey@eecs.berkeley.edu

One of the major challenges towards scaling electronic devices to the nanometre-size regime is attaining controlled doping of semiconductor materials with atomic accuracy, as at such small scales, the various existing technologies suffer from a number of setbacks. Here, we present a novel strategy for controlled, nanoscale doping of semiconductor materials by taking advantage of the crystalline nature of silicon and its rich, self-limiting surface reaction properties. Our method relies on the formation of a highly uniform and covalently bonded monolayer of dopant-containing molecules, which enables deterministic positioning of dopant atoms on the Si surfaces. In a subsequent annealing step, the dopant atoms are diffused into the Si lattice to attain the desired doping profile. We show the versatility of our approach through controlled p- and n-doping of a wide range of semiconductor materials, including ultrathin silicon-on-insulator substrates and nanowires, which are then configured into novel transistor structures.

Scaling device dimensions down to the molecular regime presents fundamental and technological challenges for fabricating well-defined structures with controlled atomic composition[1–9]. One proposed route for achieving such fine control is the integration of self-limiting and self-assembly processes where surface and chemical phenomena guide the synthesis and fabrication of the desired nanostructures[10–12]. Currently, there is a tremendous need for a new technology to demonstrate reliable nanoscale doping of Si structures, mainly for well-defined and uniformly doped ultrashallow junctions at the source and drain extension regions[1,2]. The conventional ion implantation process, which relies on the bombardment of semiconductors with energetic ions, suffers from (1) the inability to achieve an implantation range and abruptness down to the nanometre range, (2) stochastic spatial distribution of the implanted ions, (3) incompatibility with nanostructured materials, such as one-dimensional (1D) nanowires and (4) severe crystal damage[1–4]. On the other hand, the solid-source diffusion process lacks the desired uniformity and control over the areal dose of the dopants to be used for miniaturized device fabrication. To overcome the difficulties of the conventional technologies, tremendous research efforts have been taken in recent years to develop new strategies for introducing dopants into semiconductor materials[13–17]. Here, we present a facile and reliable approach for controlled doping of nanostructured devices by using the rich surface chemistry of crystalline silicon combined with a self-limiting monolayer formation reaction.

The monolayer doping (MLD) strategy that we present here is based on (1) the formation of self-assembled monolayers of dopant-containing molecules on the surface of crystalline Si followed by (2) the subsequent thermal diffusion of dopant atoms via rapid thermal annealing (RTA) (Fig. 1). This approach benefits from the well-defined and deterministic positioning of covalently attached monolayers featuring chemically substituted dopant atoms on the silicon surface. In a following step, the reacted interface is exposed to RTA, which results in the breakage of the molecular structures and the thermal diffusion of dopant atoms to desirable depths.

The MLD process is applicable for both p- and n-doping of various nanostructured materials that are fabricated by either the 'bottom-up' or 'top-down' approaches, making it highly versatile for various applications. An important characteristic of the method is that it uses self-limiting reactions to form a highly uniform monolayer on the pristine crystalline silicon surface, resulting in a well-defined layer of chemically attached dopant-containing molecules with molecular accuracy. This is crucial for the well-controlled and uniform formation of the nanoscale doping profiles in the following RTA step. Furthermore, the areal dopant dose is tuned by the molecular footprint of the precursor, with the smaller molecules enabling a higher dose, whereas the RTA time and temperature govern the precise nature of the junction depth. As a result, the combination of the RTA condition and the molecular design of the precursor provides a wide spectrum of doping profiles to meet the specific needs of the desired application.

Covalently anchored monolayers of boron (B)-containing molecules were formed on the surface of nearly intrinsic Si(100) by thermal activation using mild reaction conditions following the method of Sieval et al.[18] (Fig. 1). The native SiO_2 layer was removed by a treatment with 0.5% HF to form hydrogen-terminated silicon surfaces. The samples were then immediately reacted with allylboronic acid pinacol ester (Aldrich) as the B-containing reagent and mesitylene as the solvent (1/4, v/v) for 2.5 h at 120 °C, resulting in direct Si–C covalent bond formation at the C=C molecular sites. Sample preparation was carried out in a glove box with a dry N_2 environment, and all reactions were carried out under argon
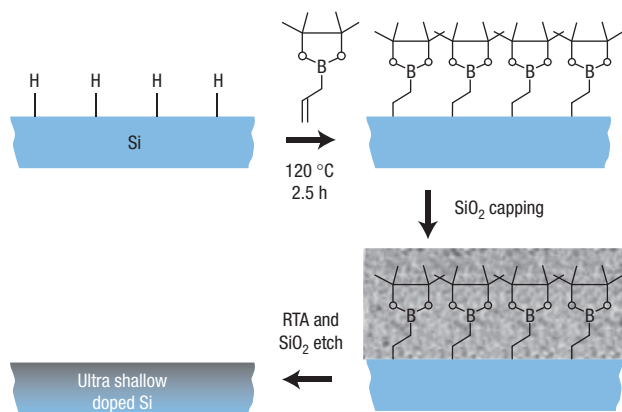
Figure 1 **Schematic diagram of the monolayer doping process for Si substrates.** The native silicon oxide layer is first removed by HF etching followed by a reaction with dopant-containing molecules to form a covalently bonded monolayer. A silicon dioxide capping layer (~50 nm thick) is then formed followed by RTA for dopant diffusion. Finally, the capping layer is removed by HF etching.

Figure 2 **X-ray photoelectron spectra of the Si 2p core region for an as-made (after 1 day exposure to ambient air) monolayer of the boron-containing compound and unreacted silicon with a native oxide layer (inset).** Peak positions I and II indicate the Si–C and Si–O binding energies, respectively.

bubbling to ensure an oxygen-free environment. On completion of the reaction, the samples show strong resistance towards surface oxidation owing to the stability of the covalently bonded monolayers, therefore enabling easy handling of the substrates[19–21]. The samples were then capped with an ~50-nm-thick SiO$_2$ layer using an electron beam evaporator. Subsequently, RTA with various temperature and time conditions was applied as a diffusion step for the dopants.

The formation of a covalently bonded monolayer using the described reaction (Fig. 1) was confirmed by X-ray photoelectron spectroscopy. As shown in Fig. 2, the Si 2p binding energy region of the reacted wafers exhibits predominately the non-oxidized Si peak, indicating a passivated surface consisting mainly of Si–C bonds. In contrast, untreated wafers with native oxide show a clear peak corresponding to the oxidized Si binding energy region. The weak shoulder observed for the passivated sample may be attributed to the slow oxidation of the monolayer-reacted substrate because of microscopic pinholes or partial degradation of the monolayer on exposure to ambient atmosphere for approximately 24 h. In the future, monolayer stability towards oxidation may be further enhanced by using long-chain-substituted dopant molecules[21]. The prevention of intervening native oxide layer formation between the dopant-containing monolayers and the Si surface is highly beneficial for the efficient diffusion of dopant atoms into the silicon crystal during the RTA step. The monolayers were further characterized by ellipsometry measurements showing a film thickness of 1.1 ± 0.2 nm, which is in good agreement with the predicted molecular length of ~0.9 nm.

Secondary-ion mass spectrometry (SIMS) measurements were carried out on the MLD-processed samples to characterize the doping profiles of the thermally diffused boron atoms (see the Methods section). Figure 3a shows a representative B doping profile obtained by MLD of a near-intrinsic Si substrate with 5 s RTA at 950 °C (blue line) and 1,000 °C (grey line). Both samples exhibit a boron concentration of $\sim 5 \times 10^{20}$ cm^{-3} near the surface, which sharply decreases to 10^{17} cm^{-3} at depths of ~18 and ~43 nm for the 950 and 1,000 °C RTA conditions, respectively. The observed 'kink-and-tail' feature arises from the reduced diffusivity of B at the high concentration limit (that is, $> 5 \times 10^{19}$ cm^{-3}), which is also a common characteristic for the conventional doping strategies[22]. The temperature dependence of the doping profiles can be well
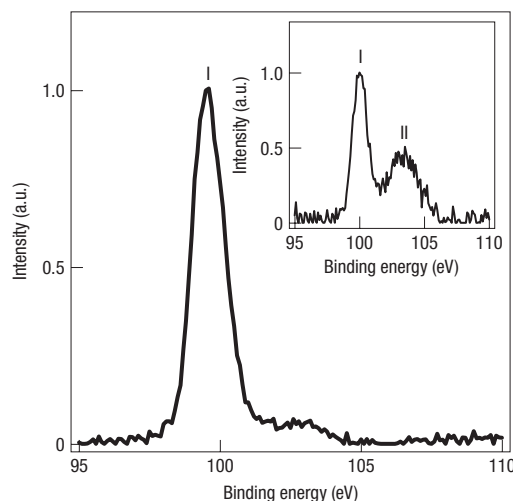
explained by the enhancement of the diffusivity constant of B at elevated temperatures. If desired, the junction depths can be further reduced by using lower annealing temperatures. Our results show that the doping profiles can be readily tuned through optimization of the RTA conditions, with nanoscale junction depths for the low annealing temperatures and short times. Notably, the high surface doping density with sharp spatial decay, obtained by using our method, is of particular interest for the formation of ultrashallow junctions at the source/drain extensions of nanoscale devices[1,2].

To further characterize the MLD samples, four-point probe measurements were carried out to obtain the sheet resistance, R_s, at various RTA conditions. Figure 3b shows the R_s values of boron-monolayer-doped Si substrate as a function of annealing time and temperature. As expected, R_s values sharply decrease from $\sim 10^5$ to $\sim 10^3$ $\Omega / \square$ after 20 s RTA at 1,050 °C, corresponding to the rapid diffusion of B atoms from the surface into the Si lattice, with the decrease in resistance approaching saturation for longer annealing times owing to the limited B source. Whereas for an annealing time of <20 s, the decrease in the resistivity is less prominent with decreasing annealing temperature (that is, 1,000 °C and 950 °C), for a long annealing time, the sheet resistance values of the three temperatures nearly converge. This trend is well explained by the lower diffusivity of B atoms at lower temperatures and fits the predicted 'limited source' model. Assuming a fully formed monolayer and using a molecular footprint of ~0.2 nm^2, the expected number of B atoms on the surface before RTA is $\sim 4.9 \times 10^{14}$ cm^{-2}, which corresponds to the maximum possible areal dose (see the Supplementary Information). From the annealing time evolution of R_s for 1,050 °C RTA, we deduce an experimentally attained boron dose of $\sim 1.7 \times 10^{14}$ cm^{-2}, which suggests an efficiency of ~33% in the number of B atoms that are effectively diffused into the Si substrate after RTA (see Supplementary Information, Fig. S1). We speculate that the 'lost' boron atoms diffused into the evaporated SiO$_2$ capping layer during the RTA step. As expected, when the MLD process was carried out without the SiO$_2$ layer, a substantial decrease (approximately 2 times for 950 °C RTA) of the doping efficiency was observed, which corresponds to the enhanced escape of the dopants from the surface and into the ambient environment.
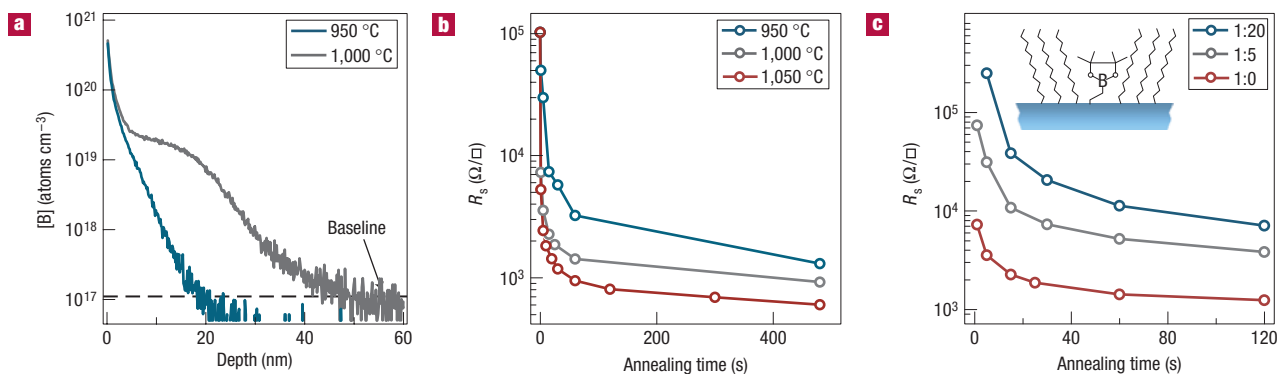
Figure 3 Boron monolayer doping (p-doping) of Si(100). **a**, SIMS profile for 5 s annealing at 950 and 1,000 °C. **b**, Sheet resistance versus time at different RTA temperatures. **c**, Sheet resistance versus time for different boron and blank molecular precursor mixing ratios, showing controlled modulation of the B dose (RTA temperature 1,000 °C). Inset: Schematic diagram of a dodecene and allylboronic acid picanol ester mixed monolayer.

In future, the doping efficiency can be further improved by using a more dense oxide capping material, such as a chemical vapour deposited oxide.

Importantly, repeating the same MLD procedure with hexylboronic acid picanol ester, the saturated analogue of allylboronic acid pinacol ester, as the precursor does not result in an observable doping effect (see Supplementary Information, Fig. S2). This result is indicative of covalently bonded monolayer formation on the Si surface involving the C=C site of the B precursor without any significant physisorbed species. As a monolayer is used, the junction depth and areal dose can be easily and accurately controlled with high uniformity. Notably, the standard deviation in the measured R_s values across an entire 10 cm^2 substrate for any given RTA condition is only 2–5%, demonstrating the high uniformity of the nanoscale doped surfaces with high reproducibility from sample to sample.

An important outcome of the use of the substrate surface chemistry is the ability to readily control the areal dose of the dopants by forming a mixed monolayer of 'blank' and dopant-containing molecules. To demonstrate dose modulation using our approach, we reacted the Si substrate with a mixture of allylboronic acid pinacol ester (B precursor) and dodecene (all-carbon 'blank' precursor) in different ratios (Fig. 3c). Dodecene is known to covalently bond to the Si surface via a chemical reaction similar to that of our B precursor, involving the C=C molecular site. As a result, dodecene effectively reduces the total Si sites available for reaction with the B precursor, therefore, lowering the areal dose of boron. The obtained sheet resistance versus time after RTA follows the expected trend with lower R_s values corresponding to the higher concentration of B precursor used in the reaction mixture (Fig. 3c). Interestingly, the experimentally extracted dose values show a direct correlation to the concentration of the B precursor in the reaction mixture, with the 1:5 and 1:20 (M:M, B/blank) mixtures showing an approximately 5- and 20-fold decrease in the dose as compared with the reaction with only B precursor (see Supplementary Information, Fig. S1b). This result suggests a similar surface reactivity for the two-terminal alkene compounds.

To further generalize our approach, we explored the doping of silicon substrates with phosphorous (P) atoms to achieve well-controlled and ultrashallow n-doped regions. Diethyl 1-propylphosphonate (DPP, Alfa Aesar) was used as the molecular precursor containing a P atom. Although the precise nature of the bonding interactions between the phosphonate compound used here and Si substrates is not well known, we observed a saturation of dopant dose as a function of monolayer reaction time for $t > 10$ min, suggesting that the surface reaction with DPP is indeed self-limiting (see Supplementary Information, Fig. S3). We are currently exploring the specific reactions and bonding configurations that take place to shed further light on the nature of the surface chemistry of these compounds. The SIMS analysis and sheet resistivity measurements of a Si substrate ((100), intrinsic) after P monolayer doping are shown in Fig. 4a. Ultrashallow junctions with a surface concentration of ~1.0×10^{22} cm^{-3} are achieved for 5 s RTA at 950 °C, which sharply decays to 10^{17} cm^{-3} at a depth of ~30 nm. Similar to the boron data, the observed R_s values as a function of RTA time and temperature fit the expected trend from the limited-source modelling (see Supplementary Information, Fig. S4). Assuming a molecular footprint of ~0.1 nm^2 for the monolayer, we extract a doping efficiency of ~95% from the sheet resistance data, corresponding to a total P dose of 7.9×10^{14} cm^{-2} (see Supplementary Information, Fig. S4). The higher diffusion efficiency of P- as compared with B-MLD is in agreement with the drastic difference in the diffusivity of phosphorus (3.2×10^{-18} cm^2 s^{-1}) and boron (1.39×10^{-16} cm^2 s^{-1}) in the SiO$_2$ capping layer at 1,000 °C (ref. 23). As a result, during the RTA step, B atoms have a higher probability of diffusing into the SiO$_2$ cap than P atoms.

Besides the mixed monolayer formation, the areal dose can be readily tuned by using the molecular structure details of the dopant precursor. For instance, the molecular footprint of the precursor directly governs the surface concentration of the dopants, with larger molecules resulting in a lower dose. To demonstrate this concept, we explored P-MLD of Si by using trioctylphosphine oxide (TOP) as the precursor with an approximately sixfold larger molecular footprint than DPP. The sheet resistance measurements of the two precursors are shown in Fig. 4b, with R_s values clearly higher for the bulkier TOP precursor. The total P dose deduced from fitting the measured R_s versus time values to the limited source model is found to be ~1.3×10^{14} cm^{-2} for TOP, approximately 6 times smaller than the dose obtained from DPP (see Supplementary Information, Fig. S4). This result is in good agreement with the calculated molecular footprint for the two precursors. The ability to controllably tune the dopant dose through the structural design of the precursor presents a unique and novel aspect of the MLD process for attaining the desired doping profile.

The MLD process is highly generic for various semiconductor structures, including quasi-1D and 2D materials. As an example,
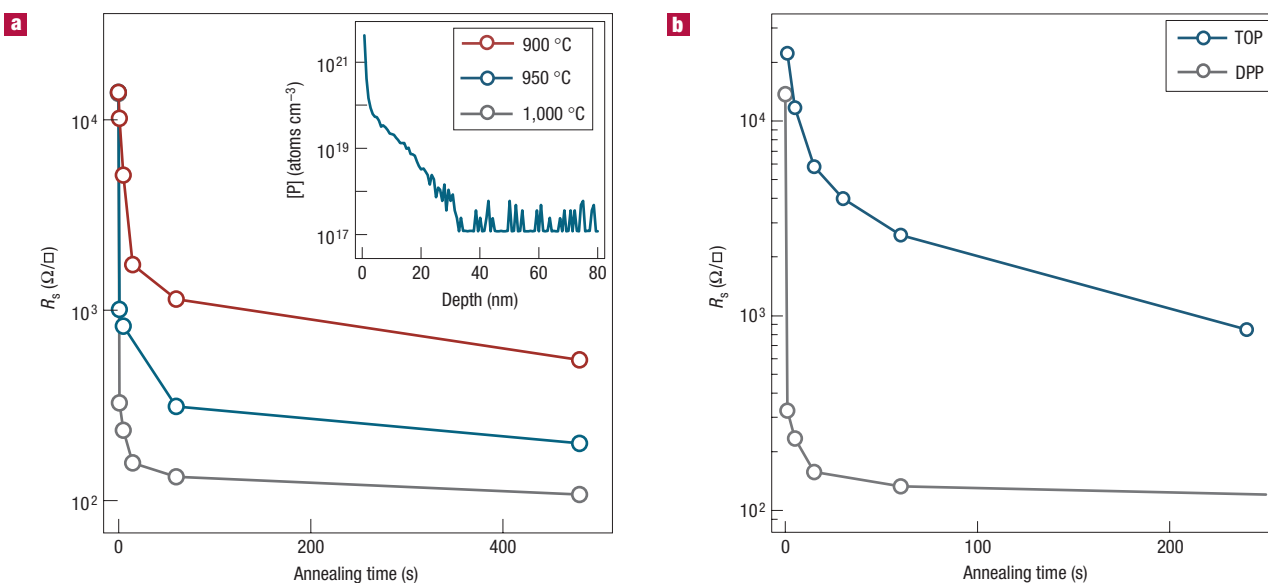
Figure 4 Phosphorous monolayer doping (n-doping) of Si. a, Sheet resistance as a function of annealing time and temperature for the DPP precursor. The inset shows the P concentration profile from SIMS for 900 °C, 5 s RTA. **b**, Sheet resistance versus time for 1,000 °C RTA for DPP (footprint ∼ 0.1 nm^2) and TOP (footprint ∼ 0.6 nm^2) precursors, showing a controlled dose modulation by using the molecular structure details of the precursor.

we applied our approach to controllably dope Si nanowires and configured them into two-terminal devices (Fig. 5a,b). Nanowires were grown intrinsically using chemical vapour deposition and Au nanoclusters[8] (30 nm). Devices fabricated using chemically intrinsic (undoped) nanowires with metal source and drain contacts (Ti/Al 5/55 nm) are highly resistive ($R \sim 100\,\text{G}\Omega$ at 1 V), which is expected owing to the large Schottky barriers arising at the nanowire–metal interfaces that limit the carrier injection. However, when the intrinsically grown nanowires are heavily n-doped using our MLD process with DPP precursor (950 °C RTA for 20 s in a N_2 atmosphere), the fabricated devices show significantly lower resistance ($R \sim 2\,\text{M}\Omega$ at 1 V) due to the thinning of the Schottky barriers at the interfaces that lead to near-ohmic contacts. Notably, such nanowires do not show any significant gate response (back-gate, ∼75 nm Si_3N_4), which is attributed to the degenerate n-doping across the entire length of the nanowire (Fig. 5b). The nanowire ($d \sim 30$ nm) doping outcome is consistent with the planar Si doping results where a depth of ∼15 nm is expected with a density of $> 10^{19}\,\text{cm}^{-3}$ for the same RTA condition. However, we speculate that for a given RTA condition, the doping profiles may not be exactly the same for nanowires and planar structures owing to the 1D nature of nanowires and the different facets involved which can affect both the diffusivity and the maximum dose. The P-MLD process was also applied to intrinsic nanowires by using the bulky TOP precursor. The TOP-doped nanowires show clear n-type switching characteristics with $I_{ON}/I_{OFF} \sim 10^3$ and $R_{ON} \sim 1\,\text{G}\Omega$, which is indicative of successful p-doping of nanowires but with lower doping density as compared with the smaller DPP precursor (Fig. 5b). The post-growth doping of 'bottom-up' nanowire materials[24] demonstrated here is of particular interest for a wide range of proposed electronic applications that incorporate nanowire building blocks[8,9,25–27]. The widely used ion implantation method is not compatible with nanowires as the energetic ions have significant probability of penetrating the entire width of a nanowire without remaining in the lattice while causing significant crystal damage[28]. On the other hand, whereas the conventional solid-source diffusion method

(that is, spin-on dopants)[29] enables doping of nanowires[9,28], its lack of control and uniformity in nanoscale presents a challenge for scaled device fabrication.

Furthermore, we applied our MLD process to ultrathin Si-on-insulator (SOI) substrates (top Si thickness ∼25 nm, with a doping density of $1 \times 10^{15}\,\text{cm}^{-3}$) to fabricate field-effect transistors (FETs) with self-aligned heavily doped Si-metal source/drain contacts (Fig. 5c). The SOI surface was first patterned using photolithography and dry etching to define the channel regions of each transistor followed by surface functionalization with a monolayer of the B-containing precursor. Tungsten (W) metal source/drain contacts were then deposited using sputtering and lift-off. A mild O_2 plasma (30 W, 30 s) step was applied, followed by a 5 s dip in 0.5% HF solution, therefore, removing the monolayer from the entire exposed Si surface while leaving the dopant-containing molecules underneath the W source/drain contacts. The subsequent RTA at 900 °C for 120 s resulted in the diffusion of B atoms, and enabled the formation of self-aligned heavily p-doped regions underneath the W contacts while maintaining the near-intrinsic nature of the channel (Fig. 5c). This self-aligned configuration is highly desirable for nanoscale devices as it enables routing of low resistive metal contacts to the edge of the channel, minimizing Schottky interfaces while lowering the parasitic resistance of the source/drain contacts as compared with the conventional metal–oxide–semiconductor field-effect transistor structures[30]. The electrical properties of the SOI FETs with a global back-gate (∼250 nm SiO_2) configuration are shown in Fig. 5d for both doped and undoped source/drain metal contacts. The impact of MLD on the FET characteristics is quite drastic with the undoped W contacts delivering ∼0.1 µA at 0.5 V compared with over 1 µA for a similar device structure but with self-aligned doped metal contacts. Furthermore, significantly better subthreshold characteristics are observed for the doped devices. The lower resistance and better switching properties are attributed to the thinning of the Schottky barriers at the metal–SOI interfaces. These results demonstrate another important aspect of the MLD scheme where the entire nanomaterial channel can be doped to
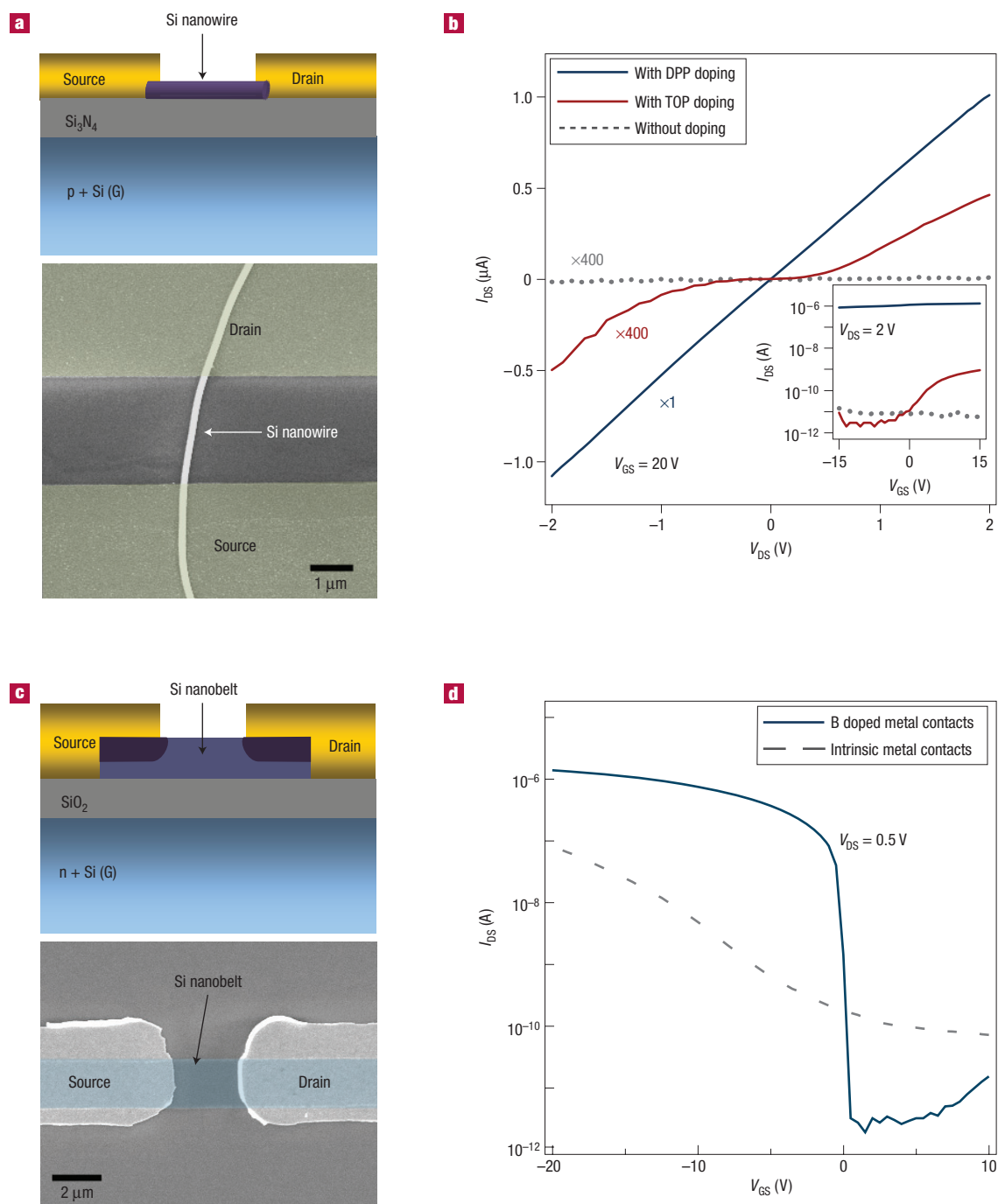
Figure 5 Monolayer doping of nanostructured Si devices. a, Schematic diagram (top) and scanning electron micrograph (bottom) of a back-gated Si nanowire device with a channel length of ~3 μm. **b**, Representative source–drain current versus voltage characteristics of intrinsically grown (undoped) Si nanowire devices with and without P-MLD of nanowires. For the P-MLD, different nanowire doping is achieved by using TOP and DPP precursors. **c**, Cross-sectional schematic diagram and scanning electron micrograph of a 25-nm-thick Si nanobelt device with W metal source/drain contacts, a global back-gate (~250 nm SiO_2), a channel width of ~2 μm and a length of ~3 μm obtained from 'top-down' patterning of SOI substrates. **d**, I–V characteristics of nanobelt devices with and without B-MLD. For the sample with MLD, a monolayer is formed only underneath the W source/drain contacts, resulting in self-aligned, heavy p-doping of the contact regions while leaving the channel near-intrinsic.

form nearly metallic structures, or the doping regions can be readily restricted to the source/drain extensions using a self-aligned process to form transistor-like devices.

In summary, we have demonstrated a novel and self-limiting approach for introducing dopant atoms to semiconductor substrates with well-defined areal dose and spatial distribution. The method is demonstrated for standard silicon substrates as well as SOI and bottom-up nanowire materials, and can be readily implemented to other types of semiconductor substrate with the appropriate surface chemistry. The applicability of

the demonstrated method to non-planar, restricted-dimension substrates such as nanowires may provide a highly desirable advance towards the fine control of the physical and electrical properties of nanomaterials for various electronic applications.

METHODS

SiO₂ CAPPING LAYER DEPOSITION

The SiO$_2$ layer was deposited by an electron beam evaporator (Edwards EB3) with a base pressure of $\sim 4 \times 10^{-6}$ torr. The chamber temperature was $\sim 50\,^{\circ}$C during the deposition process and SiO$_2$ pellets (1–5 mm, Kurt J. Lesker) were used as the evaporation source material. The evaporated SiO$_2$ film is expected to be oxygen deficient in this high vacuum environment. We note that the exact stoichiometry and composition of the capping layer can affect the diffusion efficiency of our process. In future, further enhancement of the efficiency may be attained through capping layer optimization.

SIMS MEASUREMENTS

The SIMS measurements were carried out using a Physical Electronics ADEPT-1010 quadrupole set-up. ^{10}B, ^{11}B and ^{30}Si were monitored under O$_2^+$ bombardment with an impact energy of 650 eV incident at 45°, whereas ^{30}Si and P$+^{30}$Si were monitored as negative ions under Cs$^+$ bombardment with an impact energy of 1,000 eV incident at 60°. The analysis chamber was backfilled with a partial pressure of O$_2$ to reduce ion yield variations at the surface and improve quantification. Secondary ions were collected from the centre 10% of a $450 \times 450\,\mu$ raster area. Stylus profilometry was used to determine the depth of sputtered craters and calibrate the depth scale assuming a constant sputter rate for the entire profile. Concentrations of ^{10}B, ^{11}B and P in the Si were calculated using a relative sensitivity factor determined from a standard sample. The B and P profiles were normalized on a point-to-point basis to the ^{30}Si profile before the relative sensitivity factor was applied.

References

1. Peercy, P. S. The drive to miniaturization. *Nature* **406**, 1023–1026 (2000).
2. Claeys, C. Technological challenges of advanced CMOS processing and their impact on design aspects. *VLSI Design* **2004**, 275–282 (2004).
3. Xiong, S. & Bokor, J. A simulation study of gate line edge roughness effects on doping profiles of short-channel MOSFET devices. *IEEE Trans. Electron Devices* **51**, 228–232 (2004).
4. Jones, E. C. & Ishida, E. Shallow junction doping technologies for ULSI. *Mater. Sci. Eng.* **24**, 1–80 (1998).
5. Lundstrom, M. Moore's law forever? *Science* **299**, 210–211 (2003).
6. Wong, P. H.-S. Beyond the conventional transistor. *Solid-State Electron.* **49**, 755–762 (2005).
7. Chau, R. *et al.* Silicon nano-transistors and breaking the 10 nm physical gate length barrier. *Device Research Conf.* **2003**, 123–126 (2003).
8. Lu, W. & Lieber, C. M. Semiconductor nanowires. *J. Phys. D* **39**, R387–R406 (2006).
9. Wang, D., Sheriff, B. & Heath, J. R. Silicon p-FETs from ultrahigh density nanowire arrays. *Nano Lett.* **6**, 1096–1100 (2006).
10. Chen, P. *et al.* Atomic layer deposition to fine-tune the surface properties and diameters of fabricated nanopores. *Nano Lett.* **4**, 1333–1337 (2004).
11. Parviz, B. A., Ryan, D. & Whitesides, G. M. Using self-assembly for the fabrication of nano-scale electronic and photonic devices. *IEEE Trans. Adv. Packag.* **26**, 233–241 (2003).
12. Chang, L. & Wong, P. H.-S. Diblock copolymer directed self-assembly for CMOS device fabrication. *Proc. SPIE* **6156**, 1–6 (2006).
13. Song, Y. H. *et al.* A novel atomic layer doping technology for ultra-shallow junction in sub-0.1 pm MOSFETs. *IEEE IEDM* **1999**, 505–508 (1999).
14. Kalkofen, B., Lisker, M. & Burte, E. P. Phosphorus diffusion into silicon after vapor phase surface adsorption of phosphine. *Mater. Sci. Eng. B* **124–125**, 288–292 (2005).
15. Agrawal, A. *IEEE Int. Conf. on Ion Implantation Technology Proceedings 2000* 293–299 (Alpbach, Austria, 2000).
16. Privitera, V. Ultra-low energy ion implantation of boron for future silicon devices. *Curr. Opin. Solid State Mater. Sci.* **6**, 55–65 (2002).
17. Moon, C.-R. *et al.* Application of plasma-doping technique to reduce dark current of CMOS image sensors. *IEEE Electron. Dev. Lett.* **28**, 114–116 (2007).
18. Sieval, A. B., Vleeming, V., Zuilhof, H. & Sudholter, E. J. R. An improved method for the preparation of organic monolayers of 1-alkenes on hydrogen-terminated silicon surfaces. *Langmuir* **15**, 8288–8291 (1999).
19. Filler, M. A. & Bent, S. F. The surface as molecular reagent: Organic chemistry at the semiconductor interface. *Prog. Surf. Sci.* **73**, 1–56 (2003).
20. Linford, M. R. & Chidsey, C. E. D. Alkyl monolayers covalently bonded to silicon surfaces. *J. Am. Chem. Soc.* **115**, 12631–12632 (1993).
21. Webb, L. J. & Lewis, N. S. Comparison of the electrical properties and chemical stability of crystalline silicon(111) surfaces alkylated using grignard reagents or olefins with Lewis acid catalysts. *J. Phys. Chem. B* **107**, 5404–5412 (2003).
22. Bentzen, A., Schubert, G., Christensen, J. S., Svensson, B. G. & Holt, A. Influence of temperature during phosphorus emitter diffusion from a spray-on source in multicrystalline silicon solar cell processing. *Prog. Photovolt. Res. Appl.* **15**, 281–289 (2007).
23. Susa, N., Kawagishi, K., Tanaka, N. & Nagata, K. Diffusion mechanism of phosphorus from phosphorous vapor in amorphous silicon dioxide film prepared by thermal oxidation. *J. Electrochem. Soc.* **144**, 2552–2558 (1997).
24. Byon, K., Thanm, D., Fischer, J. E. & Johnson, A. T. Synthesis and postgrowth doping of silicon nanowires. *Appl. Phys. Lett.* **87**, 193104 (2005).
25. Lieber, C. M. & Wang, Z. L. Functional nanowires. *Mater. Res. Soc. Bull.* **32**, 99–108 (2007).
26. Huang, Y. *et al.* Logic gates and computation from assembled nanowire building blocks. *Science* **294**, 1313–1317 (2001).
27. Patolsky, F., Timko, B. P., Zheng, G. & Lieber, C. M. Nanowire-based nanoelectronic devices in the life sciences. *Mater. Res. Soc. Bull.* **32**, 142–149 (2007).
28. Beckman, R. A. *et al.* Fabrication of conducting Si nanowire arrays. *J. Appl. Phys.* **96**, 5921–5923 (2004).
29. Zhu, Z.-T., Menard, E., Hurley, K., Nuzzo, R. G. & Rogers, J. A. Spin on dopants for high-performance single-crystal silicon transistors on flexible plastic substrates. *Appl. Phys. Lett.* **86**, 133507 (2005).
30. Kinoshita, A., Tanaka, C., Uchida, K. & Koga, J. *VLSI Technol. Kyoto, Japan* 158–159 (IEEE, Piscataway, 2005).

Acknowledgements

Author contributions

J.C.H., R.Y., Z.A.J., Z.F. and R.L.A. carried out the experiments. All authors contributed to designing the experiments, analysing the data and writing the manuscript.

67

Controlled nanoscale doping of semiconductors via molecular monolayers

Johnny C. Ho*†‡, Roie Yerushalmi*†‡, Zachery A. Jacobson*†, Zhiyong Fan*†, Robert L. Alley*, Ali Javey*†

Department of Electrical Engineering and Computer Sciences, University of California at Berkeley and † Materials Sciences Division, Lawrence Berkeley National Laboratory, Berkeley, CA 94720

‡ *These authors contributed equally to this work*

Correspondence to: ALI JAVEY ajavey@eecs.berkeley.edu

Supporting Information

Doping profile modeling

For a "limited source" condition, with a surface dose of N_o, the doping density can be expressed using the following equation as a function of RTA temperature and time:[S1]

$$N(x,t) = \frac{N_o}{\sqrt{\pi Dt}} e^{-x^2/4Dt}$$

Eq. S1

N: Dopant density
N_o: Surface dose
t: Diffusion time
D: Diffusivity
x: Depth

Additionally, the resistivity, ρ, and sheet resistance R_s can be described using the following:[S2]

$$R_s = \frac{\rho}{t}$$

Eq. S2

$$\rho = \frac{1}{q\mu N}$$

t: thickness of semiconductor
q: charge
μ: mobility of the carrier
N: dopant density

Finally, the mobility is a function of doping density, using the following empirical expression:[S1]

$$\mu = \mu_{min} + \frac{\mu_{max} - \mu_{min}}{1 + (\frac{N}{N_r})^\alpha}$$

Eq. S3

	Phosphorous	*Boron*
μ_{min} (cm^2/Vs)	68.5	44.9
μ_{max} (cm^2/Vs)	1414	470.5
N_r (cm^{-3})	9.20×10^{16}	2.23×10^{17}
α	0.711	0.719

Then the sheet resistance, R_s, can then be calculated as the following:

$$R_s^{-1} = \int_0^{x_H} q\mu N(x,t)dx$$

$$R_s^{-1} = \int_0^{x_H} q\left\{\mu_{min} + \frac{\mu_{max} - \mu_{min}}{1 + \left(\dfrac{\dfrac{N_o}{\sqrt{\pi Dt}}e^{-x^2/4Dt}}{N_r}\right)^\alpha}\right\}\frac{N_o}{\sqrt{\pi Dt}}e^{-x^2/4Dt}dx$$

x_H: effective thickness of the conducting layer

It is important to note that the presented equations for analysis are oversimplified with the diffusivity of the dopant atoms considered to be constant as a function of concentration. In practice, the diffusion of dopant atoms is more complex, with dependence on the impurities (such as carbon) as well as dopant concentrations.

Molecular footprint approximations, from DFT calculations, for the B and P containing molecules are used to estimate the surface dose, assuming a fully formed monolayer:

For the boron containing molecule (allylboronic acid pinacol ester):

0.21nm^2 area footprint

Surface density=4.9×10^{14}cm^{-2}

For the phosphorous containing molecule (diethyl 1-propylphosphonate):

0.12nm^2 area footprint

Surface density=8.3×10^{14}cm^{-2}

The surface density corresponds to the maximum possible areal dose of the dopants (atoms/cm^2). In theory, if all surface dopant atoms are diffused into Si during RTA, then an efficiency of 100% is attained. However, in practice, not all dopant atoms make it to the Si lattice, and instead some are lost through diffusion into the capping layer. The doping efficiency can be readily obtained from the ratio of the experimentally extracted dose by that of the expected maximum dose.
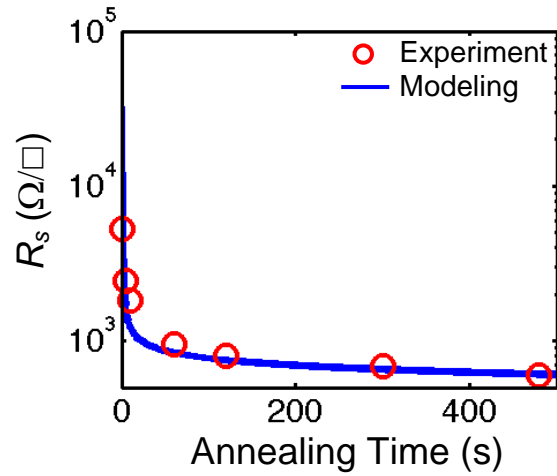
Figure S1a. Sheet resistance vs. annealing time for B-MLD (1050ºC RTA in N_2). Experimental data and modeling results (from Eq. S4) are shown. For modeling, a dopant dose $N_o=1.6 \times 10^{14} cm^{-2}$ was used to fit the experimental data. This dose corresponds to a doping efficiency of ~33%, assuming a perfect monolayer formation on the Si surface prior to RTA, and is also in good agreement with the dose that is extracted from SIMS measurements ($N_o=7.5 \times 10^{13} cm^{-2}$). The small discrepancy in the dose values obtained from the two methods may be due to the measurement uncertainty of the SIMS analysis near the Si surface.
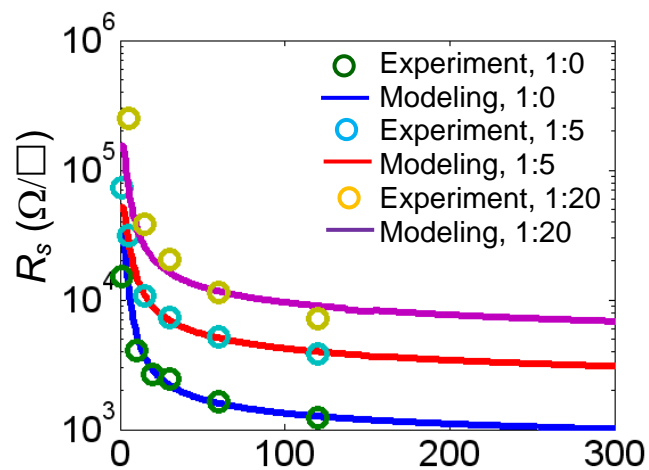
Figure S1b. Sheet resistance vs. annealing time for B-MLD (1000°C RTA in N_2). Experimental data and modeling results (from Eq. S4) are shown for various ratios of allylboronic acid pinacol ester and dodecene precursor mixtures. For modeling, a dopant dose $N_o = 4.9 \times 10^{14}$ cm^{-2}, $N_o = 1 \times 10^{14}$ cm^{-2} and $N_o = 3 \times 10^{13}$ cm^{-2} were used to fit the experimental data of 1:0, 1:5 and 1:20 (B:blank precursor ratio) mixtures, respectively.
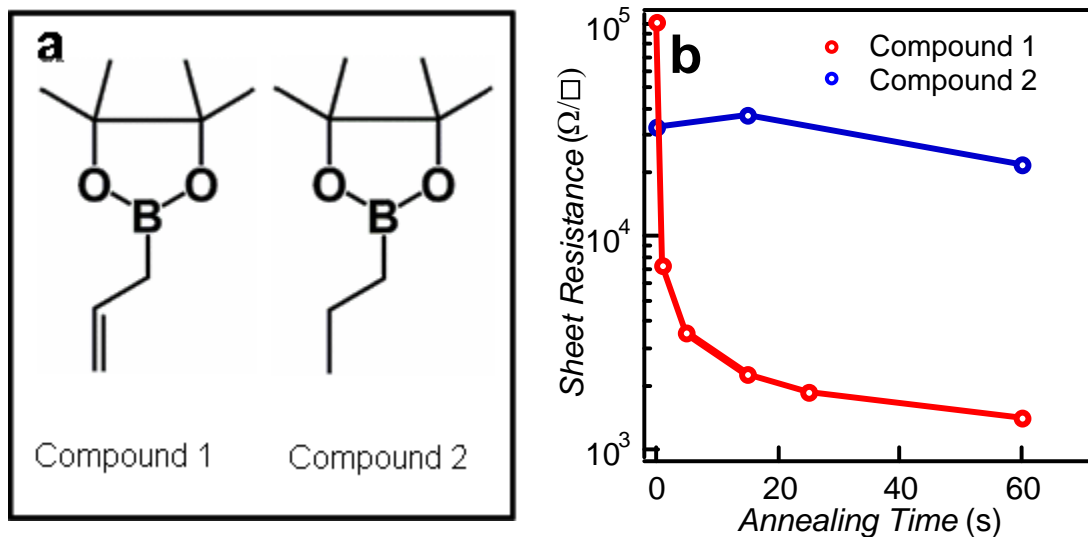
Figure S2. a, Schematics of allylboronic acid pinacol ester (compound 1) and hexylboronic acid picanol ester (compound 2) used as the B containing molecules for surface reactions. **b**, Sheet resistance vs. annealing time obtained for the two compounds with 1000°C RTA in a N_2 atmosphere. The sample treated with compound 2 does not show a clear doping effect after RTA due to the lack of formation of a monolayer for this compound during the surface reaction. This result shows the key role of the C=C molecular site of compound 1 for the formation of covalently bonded monolayer on Si surfaces, furthermore, ruling out a simple physisorption of the molecular species. The covalently bonded monolayer formation is highly desirable for achieving well controlled and highly uniform doping profiles.
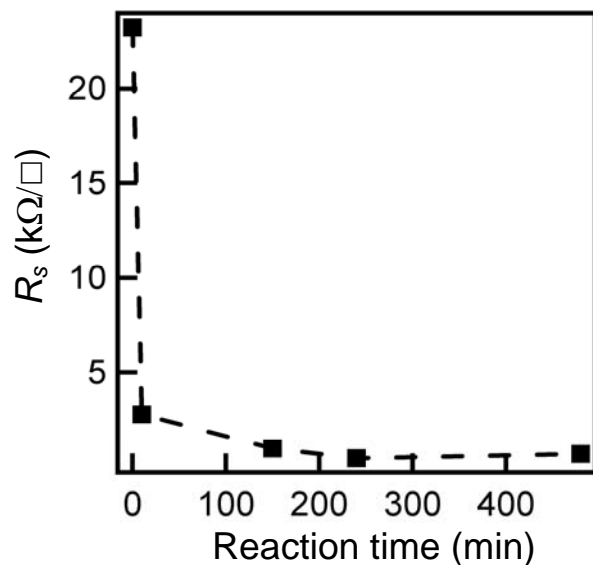
Figure S3. Sheet resistance as a function of the surface reaction time between the intrinsic Si substrate and diethyl 1-propylphosphonate, the phosphorous containing compound. After the reaction, and the deposition of a SiO_2 cap layer, RTA at $950^{\circ}C$, 15 sec in a N_2 atmosphere was conducted on each sample. The sheet resistance was then measured after the removal of the cap. It is quite evident that the sheet resistance, and therefore the P dose, saturates for reaction time longer than ~10 min. This shows that the surface reaction between the P containing molecule and Si is self-limiting, which is highly optimal for achieving a well controlled dopant dose and profile.
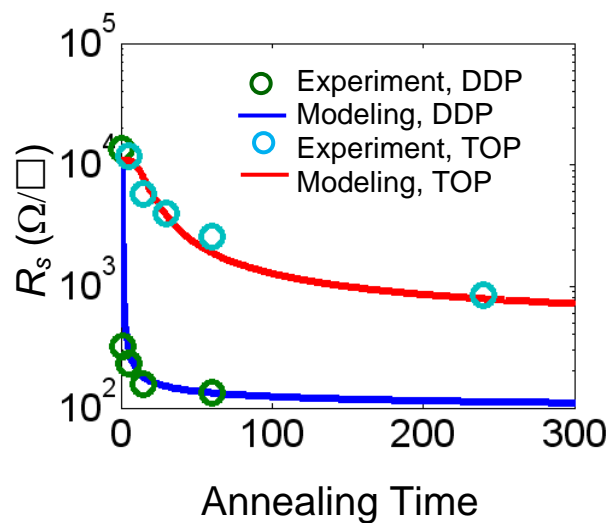
Figure S4. Sheet resistance vs. annealing time for P-MLD (1000ºC RTA in N_2). Experimental data and modeling results (from Eq. S4) are shown for both DDP and TOP precursors. From sheet resistance measurements, dopant areal dose of $N_o\sim7.9\text{x}10^{14}$ cm^{-2} and $N_o\sim1.3\text{x}10^{14}$ cm^{-2} are extracted for DDP and TOP, respectively.

References

S1. Sze, S. M. *Physics of Semiconductor Devices: Physics and Technology* 2nd ed. (Wiley, New York, 2001).

S2. Zeghbroeck, B. V. *Principles of Semiconductor Devices*, (University of Colorado, http://ece-www.colorado.edu/~bart/book/book, 2004).